Available online at www.sciencedirect.com

ScienceDirect

Ceramics International 40 (2014) 1183–1188

CERAMICS INTERNATIONAL

www.elsevier.com/locate/ceramint

Effect of substitution of magnetic rare earth Nd at non-magnetic La site on structure and properties of $LaSrFeO_4$

Devinder Singh*, Suram Singh, Arun Mahajan, Nisha Choudhary

Department of Chemistry, University of Jammu, Jammu 180006, India

Received 20 May 2013; received in revised form 23 June 2013; accepted 1 July 2013
Available online 6 July 2013

Abstract

K_2NiF_4 phases $La_{1-x}Nd_xSrFeO_4$ ($x=0.0$, 0.3, 0.6, and 0.9) have been successfully prepared by solid-state reactions. Rietveld refinement shows that all the phases crystallize in tetragonal K_2NiF_4 structure (space group *I4/mmm*). The change in the lattice constants was interpreted in terms of the ionic radius of the substituted ion. The variation of inverse molar susceptibility with temperature follows the Curie–Weiss law. The dominant magnetic interactions in the materials are antiferromagnetic, which could be due to Fe^{3+}–O–Fe^{3+} superexchange coupling. All the samples were semiconducting over the temperature range from 150 to 350 K and the resistivity data has been best fitted using the Arrhenius equation, $\rho=\rho_0 \exp(-E_a/k_BT)$.

Keywords: A. Solid-state reaction; B. X-ray method; C. Magnetic properties; C. Electrical properties

1. Introduction

The increased interest towards $LaSrFeO_4$ is invoked by the possibility of using this material as a cathode in solid oxide fuel cells (SOFC), operating at high temperature. The compound possesses high electron-ion conductivity, significant oxygen diffusion, thermo-mechanical stability and other properties suitable for SOFC cathode application. The compound crystallizes in K_2NiF_4-type structure and constitutes a particular case of the Ruddlesden–Popper phases $A_{n+1}B_nO_{3n+1}$ with $n=1$. The atomic and magnetic structure of $LaSrFeO_4$ were first studied by Souberoux et al. using X-ray diffraction, Mössbauer spectroscopy and neutron diffraction in the polycrystalline state [1]. The magnetic order was determined to be antiferromagnetic with a Neel temperature $T_N=380$ K with a saturation moment of 4.6 μ_B for the high spin state of the $3d^5$ ionic configuration of Fe^{3+}. Small differences in lattice parameters observed by different groups were attributed to the presence of traces of Fe^{4+} in the compound. The effect of hole doping on the electrical transport and magnetic properties was studied in detail by Omata et al. by introducing excess oxygen atoms [2] and by varying the Sr concentration as $Sr_{1+x}La_{1-x}FeO_4$ for $0.0\leq x\leq 0.3$ [3]. The effect of hole doping was to decrease the resistivity by three orders of magnitude at room temperature but unlike the copper based perovskite oxides the conduction behavior remained semiconducting with a decrease in band gap with increase in doping level.

There are some conflicting reports about the cell parameters and electrical resistivity of $LaSrFeO_4$. The cell parameters were reported to be $a=3.87$ Å and $c=12.7$ Å [1]; $a=3.876$ Å and $c=12.713$ Å [4]; and $a=3.8694$ Å and $c=12.7322$ Å [5]. It was reported by King et al. [6] that at room temperature $LaSrFeO_4$ with Fe^{3+} ion is semiconducting with a resistivity of 2.4×10^3 Ω cm, while Kozuka et al. [4] reported the resistivity 1.15×10^5 Ω cm, which is about 50 times greater than the former. Keeping in view of some conflicting reports about cell parameters and electrical resistivity and to study the effect of magnetic rare earth Nd at La site on the structure and properties of $LaSrFeO_4$, the phases $La_{1-x}Nd_xSrFeO_4$ ($x=0.0$, 0.3, 0.6, and 0.9) have been prepared by the solid state reaction method. Their structure was refined by the Rietveld method. The electrical transport and magnetic properties of the phases have been studied as a function of temperature.

2. Experimental

La_2O_3, Nd_2O_3, $SrCO_3$ and Fe_2O_3 (all were Aldrich made, purity 99.9%) were used as starting materials. Prior to use,

*Corresponding author.
E-mail address: drdssambyal@rediffmail.com (D. Singh).

0272-8842/$ - see front matter © 2013 Elsevier Ltd and Techna Group S.r.l. All rights reserved.
http://dx.doi.org/10.1016/j.ceramint.2013.07.003

La_2O_3 and Nd_2O_3 were calcined at 1100 °C for about 9 h in air to remove volatile impurities, $SrCO_3$ was heated at 200 °C in the oven in air to remove moisture, while Fe_2O_3 was used as received. The reactant oxides/carbonates were weighed corresponding to the stoichiometry of the phases. They were mixed and homogenized by grinding in cyclohexane using an agate mortar and pestle. The homogenized mixtures were pressed into pellets and placed in a platinum crucible and then calcined at 900 °C in static air atmosphere in an electric tube furnace for about 12 h. The calcined pellets were ground and again pressed into pellets by a hydraulic press and then calcined at 1050 °C for about 72 h with three intermittent grindings and pelletizings. Finally, the samples were cooled down slowly to room temperature in the furnace and then pulverized.

The samples were characterized by room temperature X-ray powder diffraction (XRD) measurements (Bruker AXS diffractometer type D 76181 Karlsruhe, Germany using CuKα radiations) for phase purity and crystal structure determination. The XRD patterns were obtained between 20° and 100° in steps of 0.02° with a counting time of 2 s per step and analyzed by the Rietveld refinements using the GSAS Program [7]. The morphology of the synthesized powders was determined by a scanning electron microscope (SEM) using a JEOL-JSM-6610LV with accelerating voltage 0.3–30 kV.

The oxygen content in the samples was estimated by the iodometric method. A weighed amount (0.2 g) of sample was placed in a flask and 5 ml of concentrated hydrochloric acid was added, followed by the addition of 10 ml of 10% KI solution. The volume of the solution was then raised up to 100 ml. The liberated iodine was titrated with a standard $Na_2S_2O_3$ solution. Sodium thiosulphate solution was added until the brown color of the iodine fades (light yellow). To this 1 ml of starch solution was added and the addition of $Na_2S_2O_3$ solution was continued until blue color of solution disappears. From the volume of sodium thiosulphate, which was used to titrate the solution, the amount of liberated iodine was determined. The oxygen content in the samples was then calculated from the obtained amount of iodine.

The magnetic susceptibility of the polycrystalline phases was measured by the Faraday technique in the temperature range 100–300 K using $Hg[Co(SCN)_4]$ as calibrant. All magnetic susceptibility values were corrected for diamagnetism of the constituent ions. The density of the pellets sintered at 1000 °C was determined by Archimedes' method. The electrical resistivity of the sintered pellets of the products was measured by the four probe method in the temperature range 150–350 K. For electrical contacts on the surface of the pellet, special electrodes were made by fixing thin copper wires with silver epoxy.

3. Results and discussion

XRD pattern for $La_{1-x}Nd_xSrFeO_4$ phases is presented in Fig. 1. All diffraction peaks were indexed using Sr_2TiO_4-type tetragonal structure in the space group *I4/mmm*, indicating a single phase compound. The present structure refinements for the phases were carried out using the tetragonal unit cell in the space group *I4/mmm*. The background Rietveld refinement was

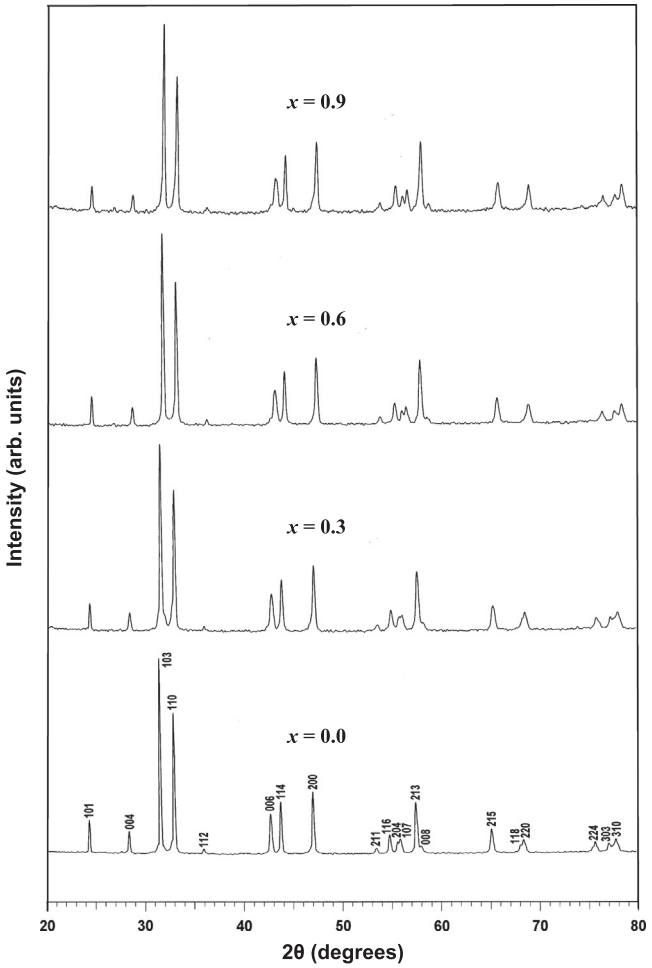

Fig. 1. X-ray diffraction pattern of $La_{1-x}Nd_xSrFeO_4$.

fitted with a shifted Chebyschev polynomial function, and a pseudo-Voight function was employed to model the peak shapes in all cases. The initial positional parameters were obtained from the data previously reported for Sr_2TiO_4 [8]. Isotropic thermal displacement parameters, initially set at 0.025 Å^2, were refined first for the metal atoms and then for the oxygen atoms with full occupancy. The occupation factors for the metals were fixed by taking sample stoichiometry into account, assuming that the La/Nd/Sr cations were randomly distributed over the 4e site while those of oxygen atoms were refined. No evidence of oxygen non-stoichiometry could be obtained from the XRD structural refinements and the oxide ion sites were therefore fixed at full occupancy. The Rietveld plot of $LaSrFeO_4$ phase is shown in Fig. 2, while the final refinement values of the structural parameters and *R*-factors in the Rietveld analysis are given in Table 1. The values of R_p, R_{wp} and χ^2 confirmed the formation of the phases. The unit cell structure of $LaSrFeO_4$, as drawn with the software "DIAMOND", is shown in Fig. 3. The data in Table 1 suggest that both the unit cell parameters *a* and *c* and cell volume decreases with increase in *x* which is consistent with the smaller size of Nd than La.

The selected bond lengths, calculated from the structural parameters, are tabulated in Table 2. The results suggest that

the apical oxygen atoms of the FeO_6 octahedra are located at the 4e site giving an Fe–O distance of 2.12720 Å, whereas the planar oxygen atoms at the 4c site are at a distance of 1.93479 Å. The local environment around the 3d transition metal site therefore consists of six oxygen atoms on the vertices of an axially distorted octahedron. The values of oxygen content in the phases determined by the iodometric method are given in Table 3. The results confirmed the presence of iron in +3 oxidation state in the samples.

The stability of $La_{1-x}Nd_xSrFeO_4$ having K_2NiF_4-type structure can be discussed in terms of the value of the tolerance factor defined by Goldschmidt [9,10] as

$$t = \frac{[(1-x)r_{La^{3+}} + (x)r_{Nd^{3+}} + r_{Sr^{2+}})/2] + r_{O^{2-}}}{\sqrt{2}(r_{Fe^{3+}} + r_{O^{2-}})}$$

The K_2NiF_4-type structure is stable over the range $0.866 \leq t < 1$. The T (tetragonal) structure exists for $0.88 \leq t \leq 0.99$ and the T/O (tetragonal/orthorhombic) structure is present for $0.866 \leq t < 0.88$.

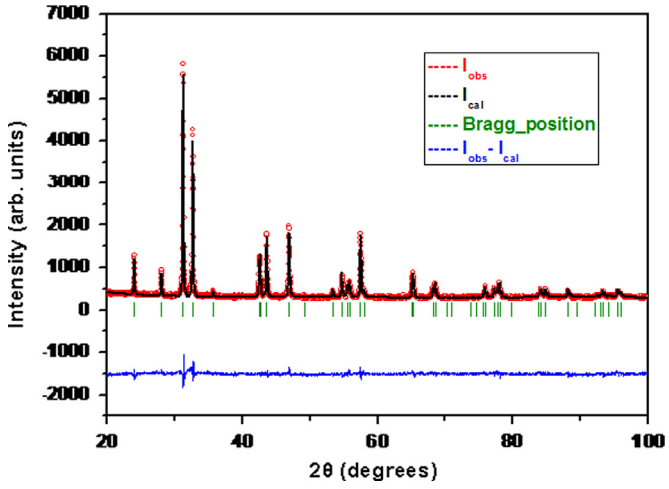

Fig. 2. Rietveld refinement profile: observed (circles), calculated (overlapping continuous line), Bragg position (vertical lines) and the difference in the observed and calculated intensities (curve at the bottom).

Based on Shannon's ionic radii [11], ($r_{La^{3+}} = 1.216$ Å, $r_{Nd^{3+}} = 1.163$ Å, and $r_{Sr^{2+}} = 1.31$ Å for CN=9; $r_{Fe^{3+}} = 0.645$ Å, in high spin state, for CN=6; and $r_{O^{2-}} = 1.40$ for CN=6), the calculated tolerance factors of the phases are given in Table 3. These values are included in the tetragonal symmetry stability range confirming the tetragonal symmetry of the proposed phases.

SEM images of the $La_{1-x}Nd_xSrFeO_4$ powders are shown in Fig. 4. It can be seen that the as-prepared samples are well

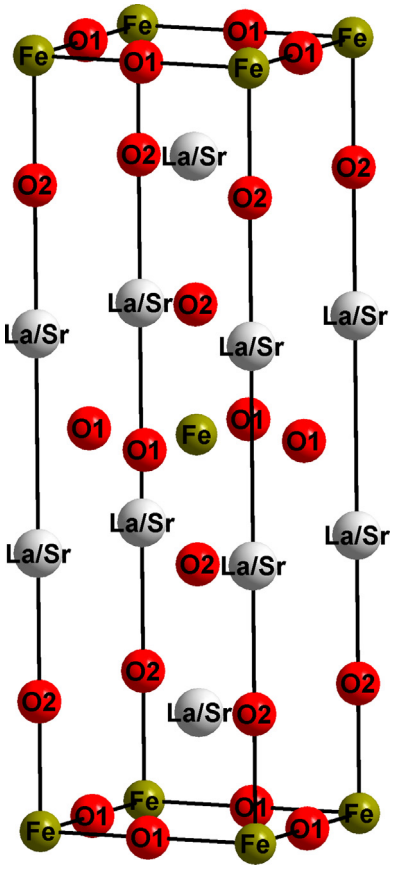

Fig. 3. Unit cell structure of $LaSrFeO_4$.

Table 1
Structural parameters obtained from the Rietveld refinement of X-ray diffraction pattern for samples $La_{1-x}Nd_xSrFeO_4$ (x=0.0, 0.3, 0.6, and 0.9). The atomic sites are: La/Nd/Sr 4e[0, 0, z]; Fe 2a[0, 0, 0]; O(1) 4c[0, 0.5, 0]; and O(2) 4e[0, 0, z] in the space group *I4/mmm*.

$La_{1-x}Nd_xSrFeO_4$		x=0	x=0.3	x=0.6	x=0.9
a (Å)		3.8695(1)	3.8617(1)	3.8537(1)	3.8493(1)
c (Å)		12.7112(3)	12.6682(6)	12.6081(6)	12.5691(8)
V (Å^3)		190.33(1)	188.92(1)	187.24(1)	186.24(1)
z	La/Nd/Sr	0.3585(1)	0.3579(2)	0.3575(2)	0.3578(3)
	O(2)	0.1673(7)	0.1637(12)	0.1687(10)	0.1696(16)
U_{iso} (Å^2)	La/Nd/Sr	0.0181	0.0146	0.0126	0.0103
	Fe	0.0210	0.0162	0.0131	0.0129
	O(1)	0.0396	0.0473	0.0161	0.0283
	O(2)	0.0276	0.0282	0.0212	0.0205
R_{wp} (%)		0.0682	0.0776	0.0639	0.0783
R_p (%)		0.0538	0.0614	0.0489	0.0608
χ^2		1.826	2.019	1.523	1.822

Table 2
Selected bond lengths of $La_{1-x}Nd_xSrFeO_4$.

Selected bond length	$x=0.0$	$x=0.3$	$x=0.6$	$x=0.9$
Fe–O(1)	1.93479(2)	1.93089(5)	1.92686(4)	1.92468(6)
Fe–O(2)	2.12720(5)	2.07321(10)	2.07321(10)	2.13142(14)
La/Nd/Sr–O(1)	2.64099(3)	2.63928(7)	2.63419(6)	2.62633(9)
La/Nd/Sr–O(2)	2.43081(5)	2.46162(12)	2.38127(11)	2.36621(16)
La/Nd/Sr–O(1)	2.75599(3)	2.74440(6)	2.74496(6)	2.74361(9)

Table 3
Tolerance factor (t), oxygen content, density, and percentage porosity of $La_{1-x}Nd_xSrFeO_4$.

x	t	Oxygen content	Experimental density (g cm^{-3})	X-ray density (g cm^{-3})	Percentage porosity
0.0	0.9209	4.002	5.61	6.04	7.12
0.3	0.9182	3.996	5.65	6.12	7.68
0.6	0.9154	3.998	5.73	6.18	7.28
0.9	0.9127	4.001	5.76	6.26	7.99

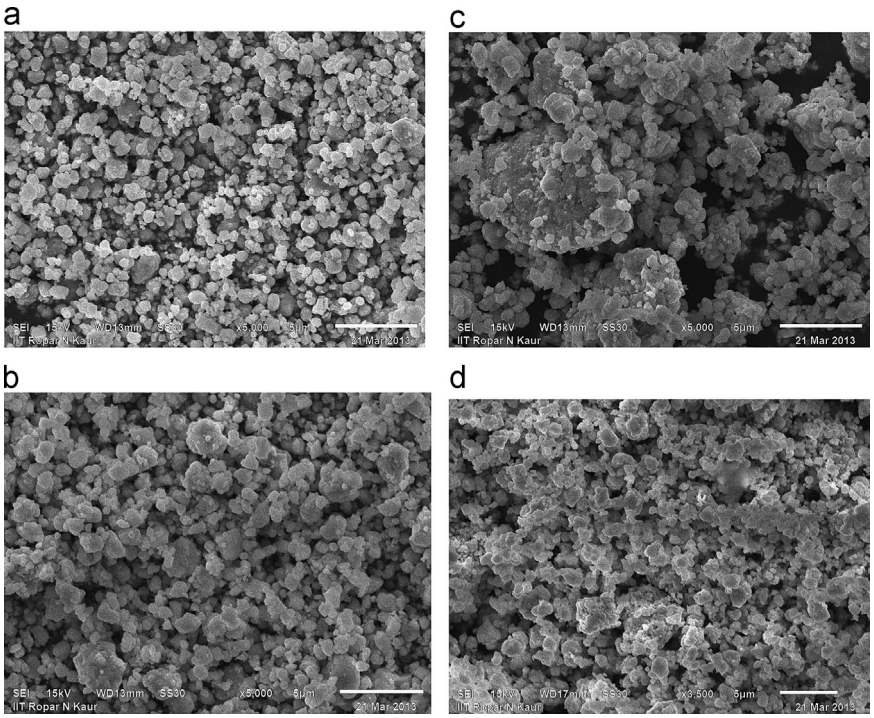

Fig. 4. SEM micrographs of $La_{1-x}Nd_xSrFeO_4$ powders (a) $x=0.0$, (b) $x=0.3$, (c) $x=0.6$ and (d) $x=0.9$.

crystallized with average grain size about 5 μm, and exhibits to a certain extent some agglomeration.

The temperature dependence of inverse molar magnetic susceptibility is shown in Fig. 5. The linearity of plots shows that the Curie–Weiss law is followed in the temperature region of investigation. The values of the Weiss constant (θ) are negative for all the materials showing the presence of antiferromagnetic interactions in them. Similar results were also reported earlier by Soubeyroux et al. [1]. The strong antiferromagnetic (AFM) coupling in the materials is readily explained by the presence of Fe^{3+}–O^{2-}–Fe^{3+}, for which AFM exchange is expected for all 180° super-exchange interactions [12,13]. The unpaired d electrons of pairs of Fe^{3+} ions will couple through covalent bonding with the p orbitals of the intervening O^{2-} ions resulting in antiparallel alignment of spins leading to antiferromagnetic behavior. When x increases, the magnetization behavior described above shows that the antiferromagnetism becomes weaker and thus spin canting of Fe moments may take place, although it is difficult to be justified from magnetization data directly. The value of the Weiss constant (θ) increases with increase in x (Table 4). The reason is that Nd

doping will possibly change the magnetic structure for Nd^{3+} cations having moments. Nd^{3+} will interact with Fe^{3+} and may influence the alignment of Fe moments, which also could result in the weakening of AFM interaction. So, with x increasing, AFM interaction is weakened and this could be the reason for the increase in the value of the Weiss constant (θ) with increase in x. Moreover, the increase in x decreases the cell dimensions more predominantly along the c-axis. In these phases, which are quasi two-dimensional in structure, interalayer magnetic interaction is usually antiferromagnetic. The weak interlayer ferromagnetic interactions are, however, strongly influenced by the decrease in the c-axis. This seems to be another reason for the increase in θ for the phases with smaller unit cell.

The effective magnetic moments (μ_{eff}), estimated from the Curie constant derived from the slope of the χ_m^{-1} versus temperature (T) plot (Fig. 5), are given in Table 4. The theoretical spin only magnetic moments for the phases have been calculated from the relationship [14]

$$\mu_{cal} = \sqrt{x\mu^2_{Nd^{3+}} + \mu^2_{Fe^{3+}}}$$

where $\mu_{Nd^{3+}}$ and $\mu_{Fe^{3+}}$ are the respective theoretical magnetic moments of Nd^{3+} (3.62 B.M.) and high spin Fe^{3+} (5.92 B.M.) ions and are given in Table 4. The smaller values of μ_{eff} than μ_{cal} could be due to the presence of antiferromagnetic interactions in the magnetic structure of these polycrystalline phases. The comparison of the $\mu_{Fe^{3+}}$ values (Table 4) shows that the contribution of the Fe^{3+} ion to the magnetic moment at 300 K increases with increasing value of x, which is attributed to decreased antiferromagnetic component in the magnetic interactions. However, in none of the phases, the $\mu_{Fe^{3+}}$ is of the order of the theoretical magnetic moment of the high spin ($t_{2g}^3 e_g^2$) Fe^{3+} ion (5.92 B.M.), which is due to the presence of antiferromagnetic interactions.

For electrical resistivity measurements, the powders were fabricated into pellets and then sintered at 1000 °C in static air atmosphere in an electric tube furnace for about 12 h. The experimental densities of the sintered pellets were about 92% of the theoretical density. The percentage porosity of the samples was also calculated using the relation [15]

$$\rho = \left[1-\left(d_{mea}/d_{cal}\right)\right] \times 100$$

where d_{mea} is the measured density and d_{cal} is the X-ray density. The measured density of the sintered pellets, X-ray density and the percentage porosity are given in Table 3. The electrical resistivity of $LaSrFeO_4$ at 300 K was found to be 7.76×10^3 Ω cm, which is some orders of magnitude higher than that reported by King et al. (2.4×10^3 Ω cm) [6]. This deviation could be attributed to the extrinsic factors like the grain size and porosity of the polycrystalline materials. The electrical resistivity of the materials decreases with the increase in x. This could be due to the reason that with increasing x, AFM interaction is weakened

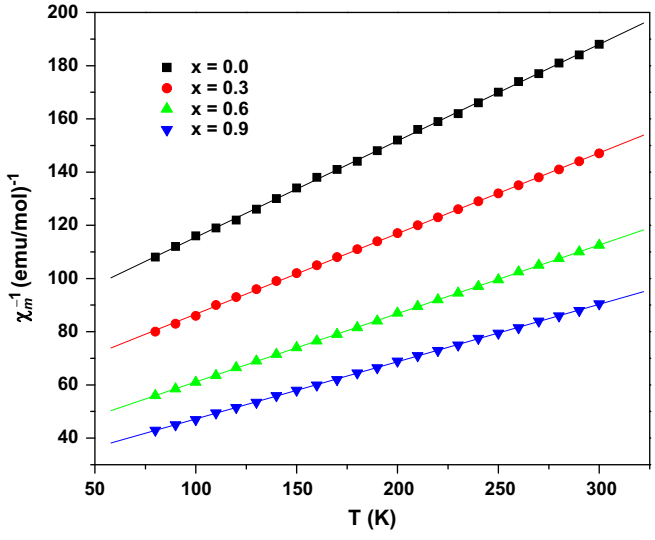

Fig. 5. Plot of inverse molar susceptibility (χ_m^{-1}) versus temperature (K) of $La_{1-x}Nd_xSrFeO_4$.

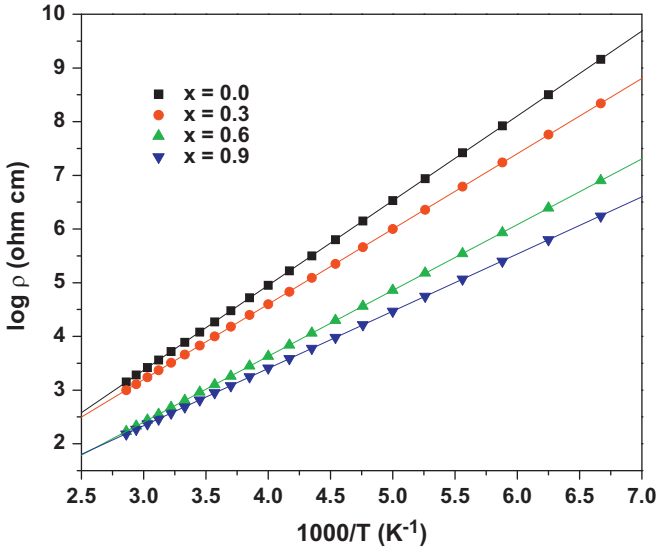

Fig. 6. Plot of log ρ versus $T^{-1/4}$ of $La_{1-x}Nd_xSrFeO_4$.

Table 4
Magnetic and electric transport data of $La_{1-x}Nd_xSrFeO_4$ giving the values of the Weiss constant (θ), the Curie constant (C), calculated spin-only magnetic moment (μ_{cal}), experimental magnetic moment (μ_{eff}), magnetic moment per Fe^{3+} ion ($\mu_{Fe^{3+}}$) at 300 K, resistivity (ρ) at 300 K, and activation energy (E_a).

$La_{1-x}Nd_xSrFeO_4$	θ (K)	C (K emu/mol)	μ_{cal} (B.M.)	μ_{eff} (B.M.)	$\mu_{Fe^{3+}}$ (B.M.)	$\rho \times 10^{-2}$ (Ω cm)	E_a (eV)
$x=0.0$	−220	2.757	5.916	4.695	3.57	77.62	0.313
$x=0.3$	−180	3.301	6.239	5.138	4.04	45.71	0.278
$x=0.6$	−136	3.885	6.547	5.574	4.62	6.456	0.243
$x=0.9$	−120	4.637	6.841	6.089	5.15	4.897	0.211

and consequently, electrons become weakly localized, the mobility of electrons is increased, resulting in the decreasing of resistivity. Various equations based upon different mechanisms of conduction, such as those applicable in case of the Arrhenius model, the Polaron hopping model and the Variable range hopping model have been applied to the data of electrical resistivity of the phases [16–18]. It was found that the resistivity (ρ) has been best fitted using the Arrhenius equation, $\rho=\rho_0 \exp(-E_a/k_BT)$, which can describe a simple semiconducting behavior. Similar results were also reported by Kozuka et al. [4] and King et al. [6]. Fig. 6 shows the Arrhenius plot of $\log \rho$ versus $1/T$ for $La_{1-x}Nd_xSrFeO_4$ phases. Since the straight line has been given by an Arrhenius plot in the temperature range employed in the present measurement as seen in Fig. 6, the apparent activation energy for conduction of the samples, E_a, can be calculated from the slope as

$$\text{slope} = E_a/2.303k_B$$

The values of activation energy, as determined from the slope of $\log \rho$ versus $1/T$, are given in Table 4. The value of activation energy for the phase $LaSrFeO_4$ is 0.313 eV which is in good agreement with that reported by Kozuka et al. (0.338 eV) [4].

4. Conclusion

$La_{1-x}Nd_xSrFeO_4$ phases having K_2NiF_4 structure have been prepared by the standard ceramic method. The Rietveld refinement of the powder X-ray diffraction data shows tetragonal symmetry with space group *I4/mmm*. The calculated tolerance factors of $La_{1-x}Nd_xSrFeO_4$ phases are included in the tetragonal symmetry stability range confirming the tetragonal symmetry of the proposed phases. The effective magnetic moments (μ_{eff}), estimated from the Curie constants derived from the slope of the χ_m^{-1} versus temperature (T) plot, come to be smaller than their theoretical magnetic moments (μ_{cal}) suggesting the presence of antiferromagnetic interactions in the phases. The resistivity data has been best fitted using the Arrhenius equation, $\rho=\varrho_0 \exp(-E_a/k_BT)$, which can describe a simple semiconducting behavior of the phases.

Acknowledgments

Authors are thankful to University Grants Commission, New Delhi for the financial support. Authors are also thankful to Prof. Ramesh Chandra, Institute Instrumentation Centre, Indian Institute of Technology, Roorkee, for recording XRD data. Thanks are also due to Dr. Harpreet Singh, Central Research Facility Section, Indian Institute of Technology, Ropar, for recording SEM.

References

[1] J.L. Soubeyroux, P. Courbin, D. Fournes, D. Fruchart, G.L. Flem, La phase $SrLaFeO_4$: structures cristalline et magnétique, Journal of Solid State Chemistry 31 (1980) 313–320.
[2] T. Omata, K. Ueda, N. Ueda, M. Katada, S. Fujitsu, T. Hashimoto, H. Kawazoe, Preparation of oxygen excess $SrLaFeO_{4+\delta}$ and its electrical and magnetic properties, Solid State Communications 88 (1993) 807–811.
[3] T. Omata, K. Ueda, H. Hosono, M. Katada, N. Ueda, H. Kawazoe, Electrical and magnetic properties of hole-doped $Sr_{1+x}La_{1-x}FeO_4$, Physical Review 49 (1994) 10194–10199.
[4] S. Fujihara, T. Nakata, H. Kozuka, T. Yoko, The effects of substitution of alkaline earths or Y for La on structure and electrical properties of $LaSrFeO_4$, Journal of Solid State Chemistry 115 (1995) 456–463.
[5] L. Dabrowski, D. Nov, V. Antonov, M.L. Machkova, S. Neov, V. Kozhukharov, Structure of $LaSrFeO_4$: neutron diffraction, Mössbauer spectroscopy and modelling, Bulgarian Chemical Communications 43 (2011) 203–209.
[6] H.W. King, K.M. Castelliz, G.J. Murphy, A.S. Rizkalla, Crystal structure and electrical resistivity of ceramics with compositions La_2MO_4, $La_{1.5}Sr_{0.5}MO_4$ and $LaSrMO_4$, Journal of the Canadian Ceramic Society 55 (1986) 10–14.
[7] A.C. Larson, R.B. Von Dreele, General Structure Analysis System (GSAS), Los Alamos National Laboratory Report LAUR, 2004, pp. 86–748.
[8] S.N. Ruddlesden, P. Popper, New compounds of the K_2NiF_4-type, Acta Crystallographica 10 (1957) 538–539.
[9] V.M. Goldschmidt, Skrifter Norske Viedenskaps-Akad., Oslo. I, Mathemat. Naturwiss. Klasse No. 8, 1926.
[10] P. Ganguly, C.N.R. Rao, Crystal chemistry and magnetic properties of layered metal oxides possessing the K_2NiF_4 or related structures, Journal of Solid State Chemistry 53 (1984) 193–216.
[11] R.D. Shannon, Revised effective ionic radii and systematic studies of interatomic distances in halides and chalcogenides, Acta Crystallographica Section A 32 (1976) 751–767.
[12] J.B. Goodenough, Magnetism and the Chemical Bond, Interscience, New York, 1963.
[13] J. Kanamori, Superexchange interaction and symmetry properties of electron orbitals, Journal of Physics and Chemistry of Solids 10 (1959) 87–98.
[14] H. Taguchi, Relationship between crystal structure and electrical properties of $Nd(Cr_{1-x}Fe_x)O_3$, Journal of Solid State Chemistry 131 (1997) 108–114.
[15] B.D. Cullity, Elements of X-ray diffraction, 2nd ed., Addision-Wesley Publishing Co., 1978.
[16] E. Bose, S. Karmakar, B.K. Chaudhuri, Small polaron hopping conduction and magnetic frustration in the electron-doped charge ordered $Ca_{0.85}La_{0.15}MnO_3$ system, Journal of Physics: Condensed Matter 19 (2007) 1–8.
[17] A.R. West, Solid State Chemistry and its Applications, John Wiley and Sons Ltd, 1987.
[18] N.F. Mott, E.A. Davis, Electronic Processes in Non-Crystalline Materials, 2nd ed., Clarendon, Oxford, 1979.